Materials Today Bio 32 (2025) 101648

Contents lists available at ScienceDirect

Materials Today Bio

journal homepage: www.journals.elsevier.com/materials-today-bio

Harnessing engineered exosomes as METTL3 carriers: Enhancing osteogenesis and suppressing lipogenesis in bone marrow mesenchymal stem cells for postmenopausal osteoporosis treatment

Tao Li [a,1], Jiangminghao Zhao [a,1], Jinghong Yuan [a], Rui Ding [a], Guoyu Yang [a], Jian Cao [a], Xiaokun Zhao [a], Jiahao Liu [a], Yuan Liu [a], Peichuan Xu [a], Jianjian Deng [a], Xinxin Miao [a,b,c,d], Xigao Cheng [a,b,c,d,*]

[a] Department of Orthopedics, The Second Affiliated Hospital, Jiangxi Medical College, Nanchang University, Nanchang, Jiangxi, China
[b] Institute of Orthopedics of Jiangxi Province, Nanchang, Jiangxi, 330006, China
[c] Jiangxi Provincial Key Laboratory of Spine and Spinal Cord Disease, Jiangxi, 330006, China
[d] Institute of Minimally Invasive Orthopedics, Nanchang University, Jiangxi, 330006, China

ARTICLE INFO

Keywords:
Postmenopausal osteoporosis
Serum exosomes
m6A RNA modification
Osteogenic differentiation
Lipogenic differentiation

ABSTRACT

Postmenopausal osteoporosis (PMOP), a prevalent skeletal disorder among women post-menopause, has emerged as a pressing global public health concern. Exosomes derived from serum have exhibited encouraging therapeutic potential in addressing PMOP, albeit with underlying mechanisms requiring deeper exploration. To elucidate these mechanisms, we devised a mouse model by surgically inducing ovariectomy and isolated exosomes from serum samples. Subsequently, we employed qRT-PCR, Western blotting, and immunofluorescence analysis to quantify relevant gene and protein expression patterns. To assess the biological effects on treated cells and tissues, we utilized ARS staining, oil red O staining, and micro-CT analysis. Additionally, we examined the METTL3/FOXO1 m6A site interaction and the FOXO1/YTHDF1 complex using dual-luciferase reporter assays and RIP assays. The m6A modification levels of FOXO1 were quantified via MeRIP-PCR. Furthermore, we engineered bone marrow mesenchymal stem cell exosomes by loading abundant METTL3 mRNA and decorating their surfaces with bone-targeting peptides. The successful synthesis and bone-targeting capabilities of these modified exosomes were validated through electron microscopy, *in vivo* imaging, and immunofluorescence staining. Our findings reveal that METTL3, in collaboration with YTHDF1 within serum-derived exosomes, enhances FOXO1 gene transcription by fostering m6A modification of FOXO1. This, in turn, promotes osteogenic differentiation of bone marrow mesenchymal stem cells while inhibiting lipogenic differentiation. Notably, our engineered exosomes, BT-oe-METTL3-EXO, not only harbor high levels of METTL3 but also demonstrate exceptional bone-targeting efficiency. *In vitro* studies demonstrated that BT-oe-METTL3-EXO significantly mitigated bone mass loss induced by ovariectomy in mice, bolstered osteogenic differentiation of mouse bone marrow mesenchymal stem cells, and inhibited lipogenic differentiation. Collectively, our research underscores the pivotal regulatory function of serum-derived exosomes in human bone marrow stem cells (hBMSCs) and underscores the promising therapeutic potential of BT-oe-METTL3-EXO for combating postmenopausal osteoporosis.

1. Introduction

Osteoporosis, a pervasive skeletal disorder, is characterized by diminished bone mass, compromised bone microarchitecture, heightened bone fragility, and predisposition to fractures. Epidemiological data from China in 2018 underscores the gravity of this issue, revealing that over half of women aged 60 and above are afflicted with osteoporosis [1]. Fractures resulting from this condition significantly

* Corresponding author. Department of Orthopedics, The Second Affiliated Hospital, Jiangxi Medical College, Nanchang University, 1 Minde Road, Nanchang, Jiangxi, China.
E-mail address: xigaocheng@hotmail.com (X. Cheng).
[1] These authors contributed equally to this work.

https://doi.org/10.1016/j.mtbio.2025.101648
Received 18 September 2024; Received in revised form 13 January 2025; Accepted 8 March 2025
Available online 20 March 2025

deteriorate patients' quality of life and can even be life-threatening. The associated complications place a substantial burden on families and society alike [2–4].

Current therapeutic strategies for osteoporosis primarily involve pharmacological interventions aimed at arresting bone loss and surgical procedures for managing fractures. However, these approaches are not without limitations. For instance, bisphosphonates, a frontline treatment, are associated with adverse effects such as muscle pain and jaw necrosis [5]. Denosumab, an effective bone resorption inhibitor, enhances bone mineral density but may lead to rebound fractures upon cessation [6]. Teriparatide, a PTH derivative, promotes osteogenesis but carries the risk of osteosarcoma and has a limited efficacy duration [7]. Consequently, the development of an effective, side-effect-free treatment strategy for osteoporosis remains a pivotal focus of research worldwide.

Exosomes, nanoscale bilayer lipid vesicles (50–150 nm in diameter), have garnered significant attention in osteoporosis therapy due to their ability to convey diverse small molecules and elicit minimal immune rejection. Studies have demonstrated their potential to guide mesenchymal stem cells (MSCs) towards osteogenic differentiation both *in vitro* and *in vivo* [8,9]. Furthermore, engineered exosomes have been designed for targeted gene therapy in osteoporosis, leveraging their low immunogenicity, biocompatibility, targeting specificity, high permeability, and stability [10,11]. Recent advancements include exosomes loaded with nucleic acids and modified with bone-targeting peptides, showcasing promising anti-osteoporotic effects [12,13].

M6A modification, the most prevalent post-transcriptional RNA modification in mammalian cells, dynamically regulates mRNA processing, translation, and degradation. Recent studies have implicated m6A methylation in osteoporosis pathogenesis, with METTL3 and METTL14, two key m6A methyltransferases, emerging as potential therapeutic targets [14–16]. However, the role of exosomes in modulating osteoporosis through M6A RNA modification remains largely unexplored.

In this study, we delve into the impact of serum-derived exosomes on osteogenic and lipogenic differentiation of bone marrow mesenchymal stem cells (hBMSCs). We aim to elucidate the mechanism underlying the role of METTL3 in exosome-mediated osteogenic and lipogenic differentiation of hBMSCs. Furthermore, we evaluate the therapeutic potential of bone-targeting exosomes enriched with METTL3 in a mouse model of postmenopausal osteoporosis induced by ovariectomy. Our findings may pave the way for the development of innovative, targeted therapies for osteoporosis.

2. Materials and methods

2.1. Patients and specimens

All patients and control subjects participating in this study were fully informed and provided written consent. The study protocols were approved by the Ethics Committee of the Second Affiliated Hospital of Nanchang University and adhered strictly to the principles outlined in the Declaration of Helsinki. Patients with osteoporosis, diagnosed based on a bone mineral density of less than −2.5 or a history of osteoporotic fracture, were recruited from the Second Affiliated Hospital of Nanchang University between March 2022 and March 2023. Exclusion criteria included: (1) poorly controlled blood pressure, (2) hyperlipidemia (total triglyceride level >2.26 mM), (3) diabetes (fasting glucose level >7.0 mM), (4) infectious diseases, and (5) other contraindications.

2.2. Isolation and characterization of serum exosomes

Exosomes were isolated from both serum and cell supernatant samples. Exosome extraction reagents (UR52151 and UR52121) were sourced from Umibio, and all isolation steps were performed according to the manufacturer's instructions. Following the drying of copper grids, the morphology of the exosomes was examined using transmission electron microscopy (TEM; H-7700, Hitachi, Japan). Nanoparticle tracking analysis (NTA; Particle Metrix, Zeta View) was employed to measure the diameter of the exosomes, and Western blotting was used to analyze the expression of exosome-specific markers (CD63, CD81, TSG101).

Table 1
si-RNA sequences.

Gene	Sense (5′-3′)	Anti sense (5′-3′)
Si-METTL3	GCUCAACAUACCCGUACUATT	UAGUACGGGUAUGUUGAGCTT
Si-FOXO1	CCCUCGAACUAGCUCAAAUTT	AUUUGAGCUAGUUCGAGGGTT
Si-YTHDF1	GGCGUGUGUUCAUCAUCAATT	UUGAUGAUGAACACACGCCTT
Si-YTHDF2	GGGAUUGACUUCUCAGCAUTT	AUGCUGAGAAGUCAAUCCCTT
Si-YTHDF3	CCACCACCAUUGGUGCAAATT	UUUGCACCAAUGGUGGUGGTT
Si-IGF2BP1	GCUCCCUAUAGCUCCUUUATT	UAAAGGAGCUAUAGGGAGCTT
Si-IGF2BP3	GCACCUCUGCGGCUUGUAATT	UUACAAGCCGCAGAGGUGCTT
Si-YTHDC1	GCAAGGAGUGUUAUCUUAATT	UUAAGAUAACACUCCUUGCTT

2.3. PKH26 staining

To investigate the uptake of exosomes by bone marrow stromal cells (BMSCs), DMEM containing PKH26 (UR52302)-labeled exosomes was used to replace the culture medium. After 24 h of incubation and fixation in 4 % paraformaldehyde, the cells were stained with DAPI. Subsequently, the cellular uptake of exosomes by BMSCs was observed under a microscope.

2.4. Cell culture

Human bone marrow stromal cells (hBMSCs) were obtained from ATCC (Manassas, USA). The cells were cultured in Dulbecco's modified Eagle's medium (DMEM; Invitrogen, Carlsbad, CA, USA) supplemented with 10 % fetal bovine serum (FBS; Gibco, Grand Island, NY, USA), 100 U/mL penicillin (Gibco, Grand Island, NY, USA), and 100 mg/mL streptomycin (Gibco, Grand Island, NY, USA). The cells were maintained at 37 °C in a 5 % CO2 environment until they reached 80 % confluence for harvesting.

2.5. Cell transfection

si-RNAs, overexpressed plasmids, and adenoviruses were purchased from Genepharma (Suzhou, China). hBMSCs were transfected with si-RNAs and plasmids using Lipofectamine 3000 (Invitrogen) according to the manufacturer's protocol. The transfected cells were collected 48 h post-transfection and subjected to further analysis. The specific si-RNAs used in this study are listed in Table 1.

2.6. Total RNA extraction and quantitative real-time PCR analysis

Total RNA was meticulously isolated from tissues or cells employing the Trizol reagent, with subsequent quantification performed using a NanoDrop Spectrophotometer (ThermoFisher Scientific, Waltham, MA, USA) to ensure precise concentration measurement. Subsequently, the isolated RNAs were efficiently converted into cDNA utilizing the PrimeScript RT reagent kit sourced from TaKaRa, Japan. For quantitative real-time PCR (RT-qPCR) analysis, the TB Green Premix Ex Taq II (TaKaRa, Japan) was paired with the ABI 7500 Real-Time PCR system (ThermoFisher, USA), ensuring high sensitivity and accuracy in gene expression profiling. Normalization of relative expression levels was achieved by referencing the stable housekeeping gene GAPDH. The specific primers employed for targeted gene amplification are comprehensively listed in Table 2. The transcriptional level of the genes of interest was rigorously analyzed utilizing the 2ˆ-ΔΔCt method, providing a robust and reliable means of quantifying gene expression changes.

Table 2
Primers sequences.

Gene	Forward Primer (5′-3′)	Reverse Primer (5′-3′)
GAPDH	GGAAGCTIGTCATCAATGGAAATC	TGATGACCCTTTTGGCTCCC
METIL3	CAGCACAGCTTCAGCAGTTCC	CGTGGAGATGGCAAGACAGA
FOXO1	GGGTTAGTIGAGCAGGTTACAC	TCCAATGGCACAGTCCTTATC
RUNX2	CTACTATGGCACTTCGTCAGGAT	ATCAGCGTCAACACCATCATT
ALP	AAGGACGCTGGGAAATCTGTG	CGTCAATGTCCCTGATGTTATGC
OPN	AGTTTCGCAGACCTGACATCC	TICCTGACTATCAATCACATCGG
CEBPα	CAAGAACAGCAACGAGTACCG	GTCACTGGTCAACTCCAGCAC
PPARγ	GCAAAGCAGAGACATCAGAAAG	AGGTGGGGTCATCATACATAGG
YTHDF1	CTCCATCTTICGACGACTTTGCT	GGTTCGCCCTCATTGTTTGTT
YTHDF2	CCAACTCTAGGGACACTCAGGAA	CCACGACCTTGACGTICCTT
YTHDF3	ATCAGAGTAACAGCTATCCAC	CCCAGGTTGACTAAATACAC
IGF2BP1	TCGTTGCAAGACCTITACCCTT	GGCAGCCACATCATTCTCATAG
IGF2BP3	ACTGCACGGGAAACCCATAG	CCAGCACCTCCCACTGTAAAT
YTHDC1	GAAGTGGAAGCTCTGCATCA	GCTTITGGCAAGAGACACATTC

2.7. Western blot analysis

Total proteins were extracted utilizing RIPA buffer, and their concentrations were accurately determined using a BCA protein assay kit. Subsequently, proteins were resolved via 10 % SDS-PAGE and efficiently transferred onto PVDF membranes. Blocking of non-specific binding sites was achieved with 5 % defatted milk, followed by overnight incubation with primary antibodies at 4 °C. After thorough washing with 1× TBST, the membranes were incubated with secondary antibodies at room temperature for 1 h. Protein bands were visualized and analyzed using the ChemiDoc Touch Imaging System (BioRad, USA) in conjunction with Image J software. The primary antibodies employed included CD63, CD81, TSG101, Runx2, OPN, ALP, PPARγ, CEBPα, METTL3, FOXO1, and GAPDH, all sourced from Proteintech and used at the specified dilutions.

2.8. Immunofluorescence staining

Cultured hBMSCs were fixed in 4 % PFA for 15 min and permeabilized before blocking with 5 % BSA for 60 min at 25 °C. Cells were then incubated overnight at 4 °C with primary antibodies against Runx2 and PPARγ. Following washes, fluorescence-conjugated secondary antibodies were applied for 60 min at 25 °C, and nuclei were counterstained with DAPI. Similarly, femur bone sections underwent fixation, decalcification, embedding, and antigen retrieval before being stained with the same primary antibodies and processed for immunofluorescence.

2.9. Bioinformatics analysis

The SRAMP database (http://www.cuilab.cn/sramp) was utilized to predict potential m6A methylation sites in FOXO1. Additionally, the STRING online tool (https://cn.string-db.org/) was employed to predict interactions between FOXO1 and other factors within its signaling pathway.

2.10. Dual-luciferase reporter assay

To validate METTL3's binding sites within FOXO1 mRNA, wild-type (WT) and mutant (MUT) sequences encompassing four predicted binding sites with combined scores over 0.85 were cloned into Pmir-GLO vectors. HBSMCs were co-transfected with these constructs and si-NC or si-METTL3 using Lipofectamine 3000. After 48 h, luciferase activity was assessed using a dual-luciferase reporter assay system (Promega), confirming METTL3's specific binding to FOXO1 mRNA.

2.11. RNA immunoprecipitation (RIP) assay

Cells were lysed in RIP lysis buffer, and magnetic beads were coated with IgG or METTL3 antibody overnight. The bead-bound complexes were isolated, and unbound materials were removed through washing. RNA co-precipitated with METTL3 was extracted using TRIzol and subjected to qRT-PCR analysis to confirm METTL3's interaction with FOXO1 mRNA.

2.12. Quantification of m6A RNA methylation

Total RNA was isolated in freshly prepared RNA fragmentation buffer, and the EpiQuik m6A RNA Methylation Quantification Kit (p-9005, Epigentek) was employed to measure m6A methylation levels. Briefly, 200 ng of fragmented RNA was loaded into wells, and capture and detection antibodies were added sequentially. The absorbance at 450 nm was measured, and m6A levels were calculated based on a standard curve, providing a quantitative assessment of m6A RNA methylation.

2.13. MeRIP-qPCR procedure

Extracted RNA was purified as previously described and fragmented by sonication on ice for 20 s. Subsequently, the purified mRNA fragments were incubated overnight with an m6A primary antibody (1:50, ab208577, Abcam), which had been pre-bound to magnetic beads (Thermo Fisher Scientific, USA). Following incubation, the beads were treated with Proteinase K (10 mg/mL) for 2 h. Subsequently, RNAs were isolated using N6-methyladenosine 5′-monophosphate sodium salt and subjected to RT-qPCR analysis for detection.

2.14. Alizarin Red S and oil red O staining

For Alizarin Red S (ARS) staining, two weeks after osteogenic induction, cells were stained with 2 % ARS (Solarbio, Beijing, China) at pH 4.2 to assess matrix mineralization. The stained cells were visualized under a microscope (Olympus), and the staining intensity was quantified using ImageJ software.

Similarly, for Oil Red O staining, cells were subjected to staining (Cyagen, Suzhou, China) after 3 weeks of lipogenic induction, following the manufacturer's protocol. The stained cells were visualized under a microscope (Olympus), and the staining intensity was quantified using ImageJ software.

2.15. Synthesis of bone-targeting peptide

The bone-targeting peptide (FITC-Ahx-Cys(Mal-PEG2K-DSPE)-SDSSD) was synthesized by Apeptides Co., Ltd. (Shanghai, China) (Fig. S3). DSPE-PEG2K-Mal (50 mg) was dissolved in a 1:1 mixture of DMF and methanol (2 mL), and FITC-Cys-SDSSD (1.1 equivalents) was added. The reaction mixture was stirred at room temperature for 12 h. The product was then dialyzed against pure water for 24 h (using a

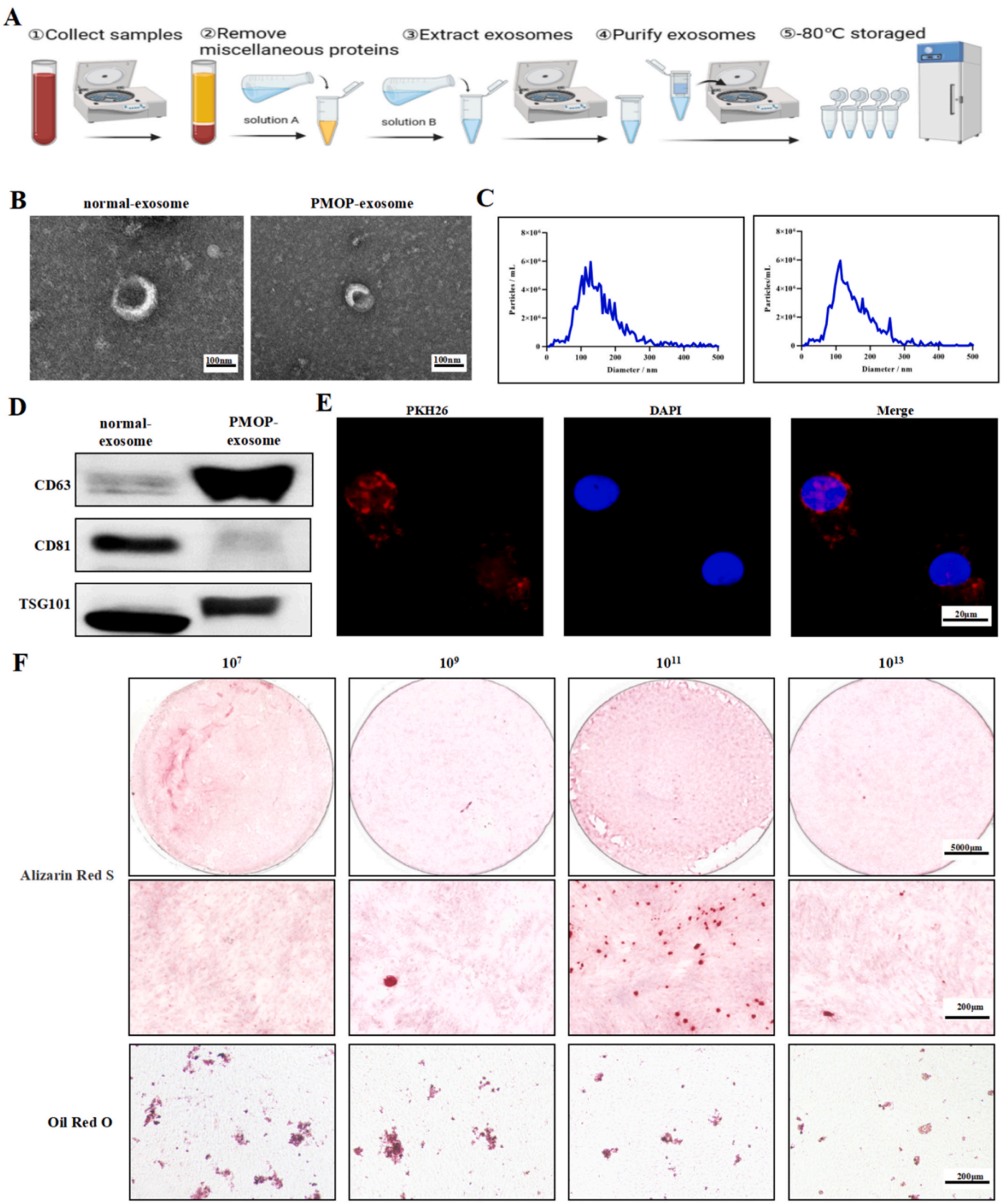

Fig. 1. Extraction and identification of exosomes. (A) Schematic diagram of exosome extraction process. (B) TEM images of normal-exosome and PMOP-exosome. (C) NTA analysis of normal-exosome and PMOP-exosome. (D) Western blot analysis of exosome-specific markers, CD63, CD81 and TSG101. (E) Exosomes from serum were labeled with PKH26 and then added to human bone marrow mesenchymal stem cells (hBMSCs). (F) Alizarin red S staining and oli red O staining of hBMSCs treated with different concentrations of normal-exosome (10^7/100μl, 10^9/100μl, 10^{11}/100μl, 10^{13}/100μl).

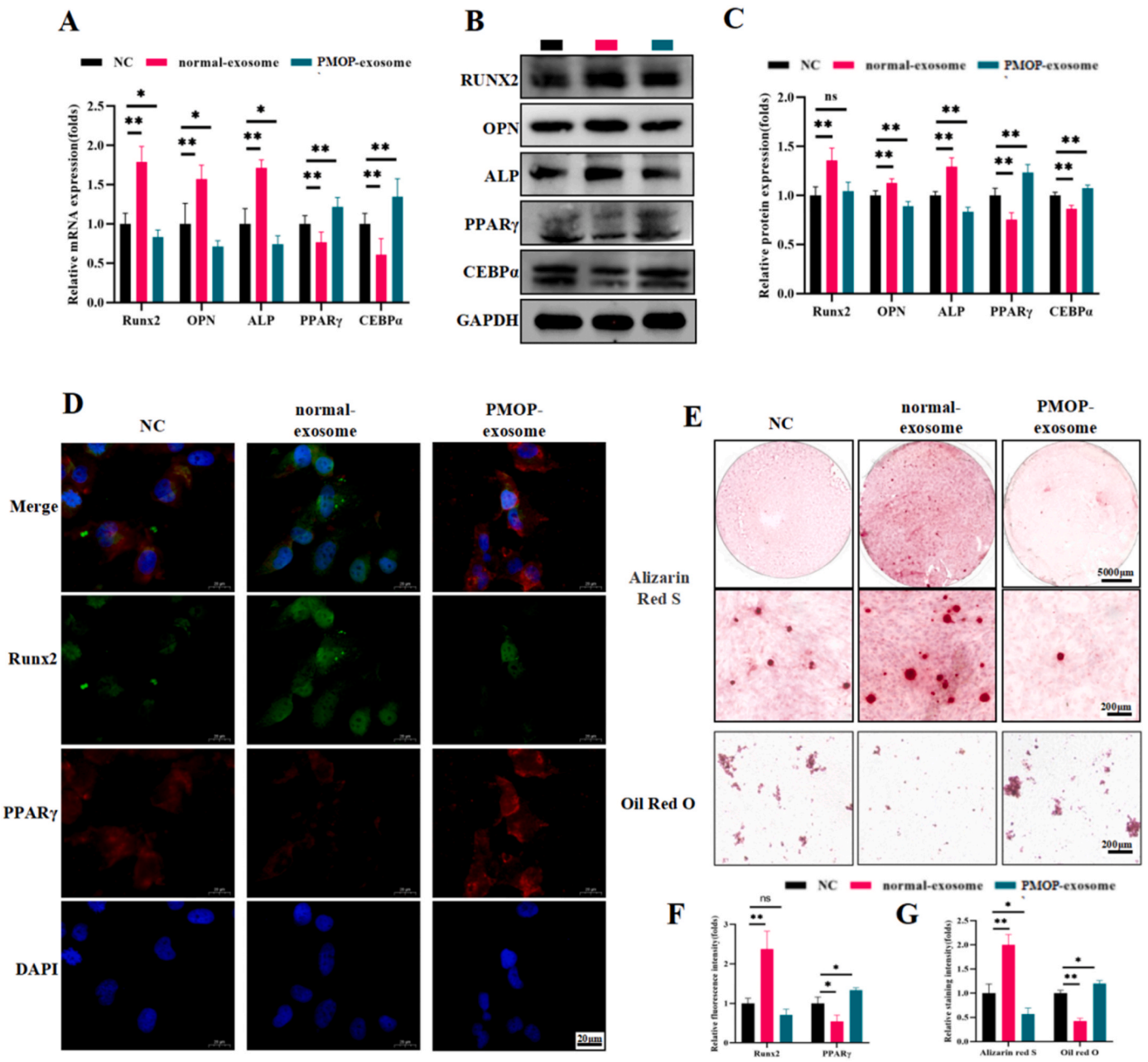

Fig. 2. Normal-exosomes promotes osteogenesis and inhibits lipogenesis in hBMSCs. (A) qPCR analysis of osteogenesis and lipogenesis-related mRNA expression in hBMSCs treated with normal-exosome and PMOP-exosome (n = 3). (B) Western blot analysis of osteogenesis and lipogenesis-related markers (n = 3). (C) Quantification analysis of osteogenesis and lipogenesis-related proteins expression. (D) Immunofluorescence of Runx2 and PPARγ in hBMSCs treated with normal-exosome and PMOP-exosome. (E) Alizarin red S staining and oli red O staining. (F) Quantification analysis of immunofluorescence of Runx2 and PPARγ(n = 3). (G) Quantification analysis of Alizarin red S staining and oli red O staining (n = 3). P values were calculated using Student's t-test. Data are expressed as the mean ± SD, *<0.05, **<0.01.

dialysis bag with a molecular weight cutoff of 2000 Da), frozen, and dried.

2.16. Synthesis of BT-oe-METTL3-EXO: oe-METTL3-EXO extraction and conjugation with bone-targeting peptide

METTL3 lentivirus was transfected into hBMSCs, and exosomes were extracted from the cell supernatant. To synthesize BT-oe-METTL3-EXO, 10 μL of exosomes and 90 μL of FITC-Ahx-Cys(Mal-PEG2K-DSPE)-SDSSD (10 μM) were mixed in 100 μL of PBS and incubated overnight at 4 °C. Unbound peptide was removed by ultracentrifugation (100,000 g, 4 °C, 70 min), and the product was resuspended in PBS.

2.17. Biophotonic imaging analysis

For *in vivo* tracking, exosomes with or without FITC labeling were intravenously injected into mice via the tail vein. For hybrid exosome tracking, 200 μL of oe-METTL3-exo or BT-oe-METTL3-exo were injected similarly. Mice were sacrificed 4 h post-injection, and relevant organs were harvested. Fluorescence imaging of the distribution was performed using a Quickview 3000 system (Bio-Real Sciences, Salzburg, Austria).

2.18. Ovariectomized animal model and experimental groups

Female C57BL/6 mice (Changsha Tianqin Biotechnology Co., Ltd.,

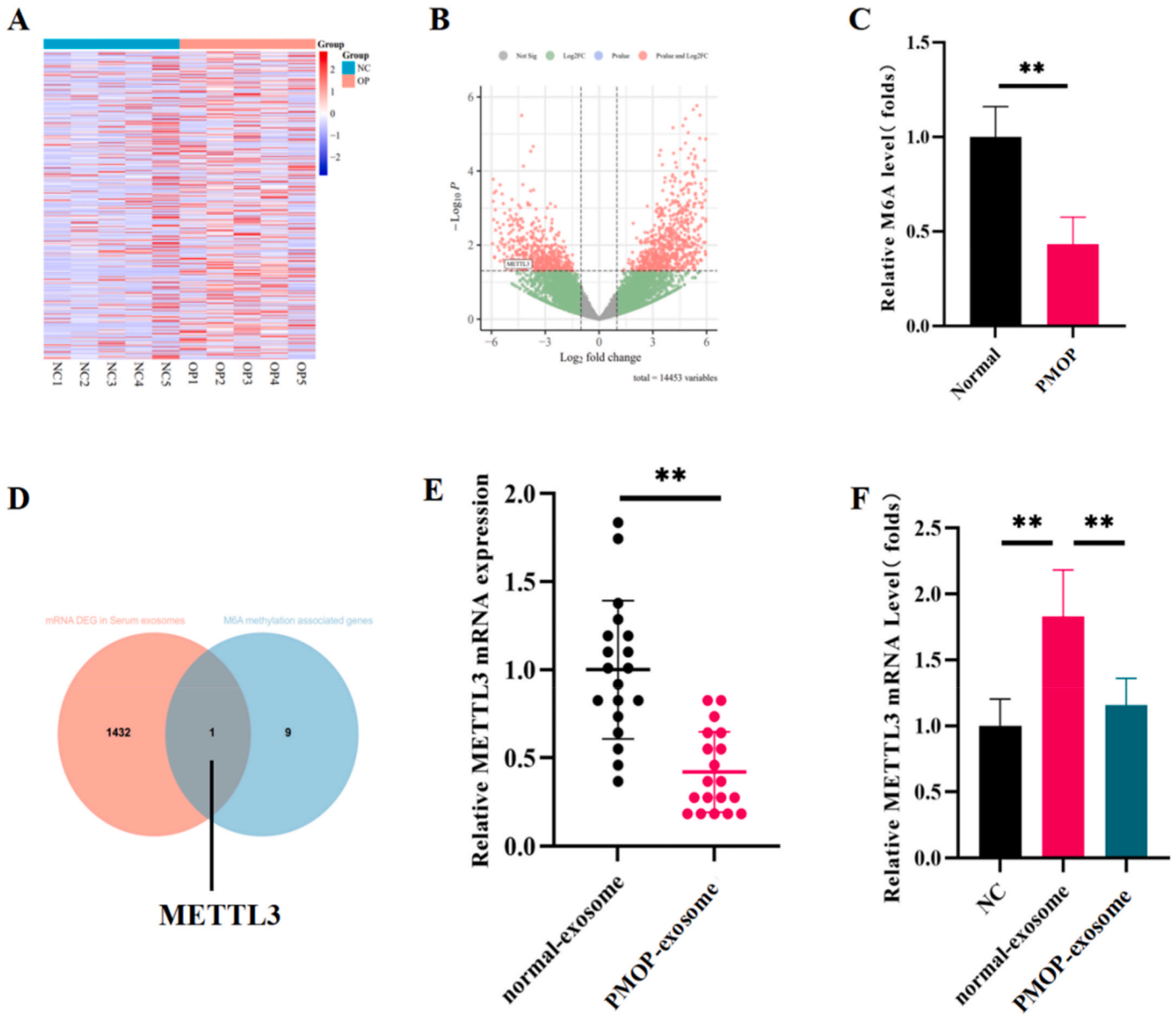

Fig. 3. METTL3 derived from serum was a candidate mRNA for postmenopausal osteoporosis. (A) Heat map showing differential mRNA expression levels (B) Volcano plot showing fold differences in gene expression and P value relationship for the significance test. (C) m6A methylation level of BMSCs from human samples (19/19). (D) Venn diagrams screen out candidate mRNA (E) qPCR analysis of METTL3 mRNA expression in human samples (19/19). (F) qPCR analysis of METTL3 mRNA expression in hBMSCs treated with normal-exosome and PMOP-exosome (n = 3). P values were calculated using Student's t-test. Data are expressed as the mean ± SD, *<0.05, **<0.01.

China) were housed in specific pathogen-free (SPF) conditions. In the first assay, 24 twelve-week-old mice were randomly divided into four groups (n = 6 per group): sham + PBS, OVX + PBS, and OVX followed by treatment with normal-exosome or osteoporosis-exosome. In the second assay, four groups were established: sham + PBS, OVX + PBS, OVX + oe-METTL3-EXO, and OVX + BT-oe-METTL3-EXO. OVX surgery was performed on all OVX groups, while the sham group underwent adipose tissue removal around the ovaries. After 6 weeks, mice in treatment groups received intravenous injections of 1 mL PBS containing 1.0×10^{11} particles per mL of the respective exosomes every two days for 6 weeks via the tail vein. Sham + PBS and OVX + PBS groups received 1 mL of PBS only.

2.19. Histological staining and analysis

Femoral and viscera specimens were fixed in 4 % paraformaldehyde at 4 °C for 24 h, followed by decalcification in 10 % EDTA at room temperature for 21 days. Samples were then embedded in paraffin and sectioned (3 μm thick) along the longitudinal axis. Femoral sections were stained with H&E and Masson's trichrome, while viscera sections were stained with H&E.

For immunofluorescence, femurs were fixed, decalcified, and embedded as above. Sections were blocked with 5 % BSA for 60 min at 25 °C, followed by overnight incubation with primary antibodies against mouse Runx2 (1:100, 20700-1-AP, Proteintech) and PPARγ (1:50, 16643-1-AP, Proteintech) at 4 °C. Fluorescent secondary antibodies and DAPI were used for staining, and sections were observed under a laser confocal microscope. Immunohistochemistry was performed similarly, using a horseradish peroxidase–streptavidin detection system for immunoreactivity.

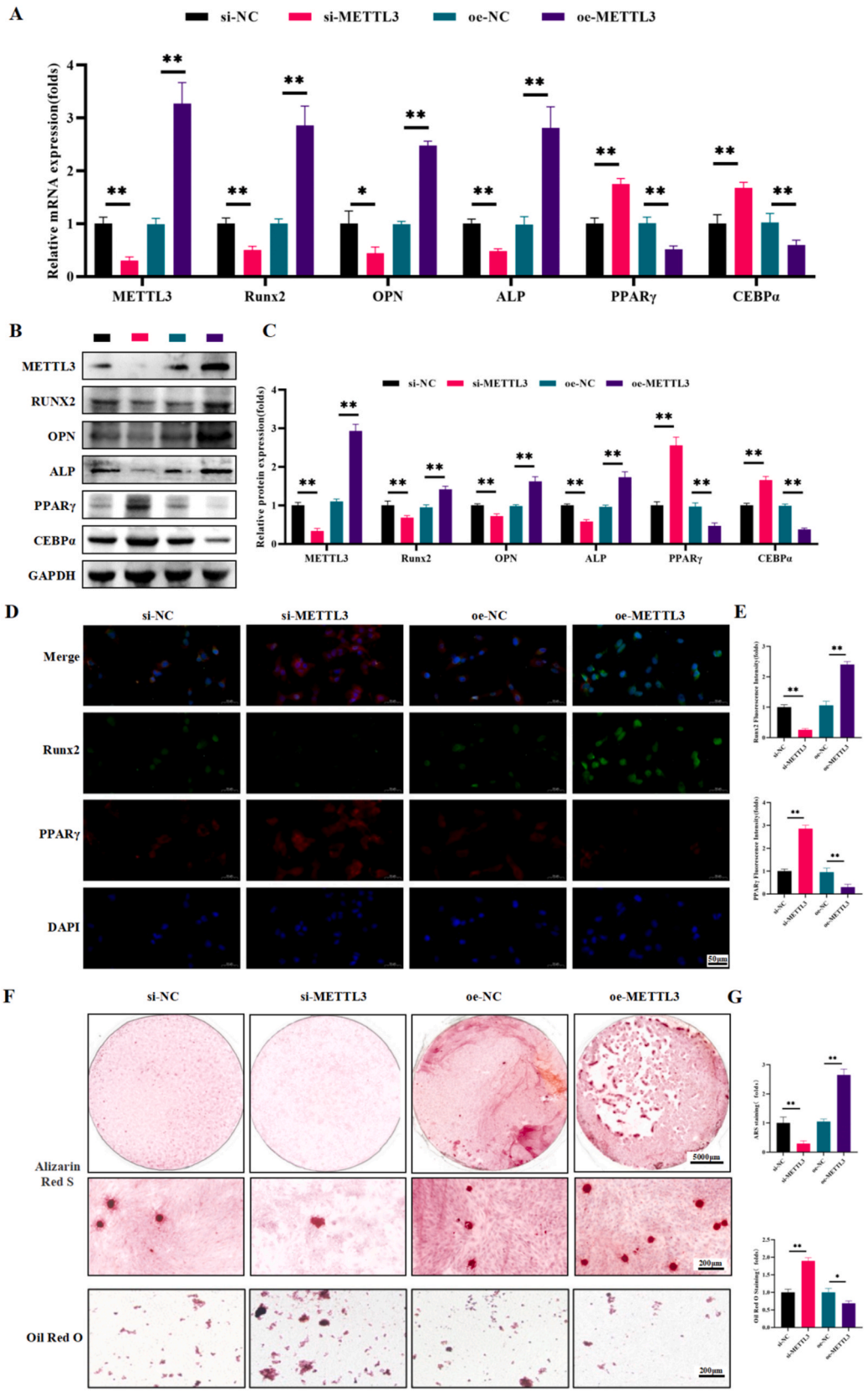

Fig. 4. METTL3 promotes osteogenesis and inhibits lipogenesis in hBMSCs. (A) qPCR analysis of METTL3, Runx2, OPN, ALP, PPARγ, CEBPα mRNA expression transfected by si-METTL3 and METTL3 overexpression plasmid (n = 3). (B) Western blot analysis of METTL3, osteogenesis and lipogenesis-related markers. (C) Quantification analysis of METTL3, osteogenesis and lipogenesis-related protein expression (n = 3). (D) Immunofluorescence of Runx2 and PPARγ in hBMSCs transfected by si-METTL3 and METTL3 overexpression plasmid. (E) Quantification analysis of immunofluorescence of Runx2 and PPARγ(n = 3). (F) Alizarin red S staining and Oli red O staining. (G) Quantification analysis of Alizarin red S staining and oli red O staining (n = 3). P values were calculated using Student's t-test. Data are expressed as the mean ± SD, *<0.05, **<0.01.

2.20. Hemolytic test

Blood samples were initially harvested from rats and subsequently centrifuged at 1500 revolutions per minute (rpm) for a duration of 15 min. The erythrocytes were then resuspended in a sterile saline solution. To establish control and experimental groups, aliquots of 50 μL of this erythrocyte suspension were mixed with either 700 μL of 0.9 % saline solution (negative control) or 700 μL of ddH2O (positive control). In the experimental group, a 700-μL mixture of 0.9 % normal saline and exosomes (oe-METTL3-EXO and BT-oe METTL3-EXO) was added to the same volume of red blood cells. All samples, contained within Eppendorf tubes, were incubated at a temperature of 37 °C in a water bath for 1 h. Following incubation, the supernatant was aspirated and its absorbance at a wavelength of 540 nm was assayed using an enzyme-linked immunosorbent assay (ELISA) reader. The resultant absorbance data were used to quantify the hemolysis rate.

2.21. Micro-CT analysis

Fixed femora were scanned using a SkyScan 1176 Micro-CT system (Bruker, Germany) at a resolution of 18 μm. Bone mineral density (BMD), bone surface (BS), bone volume fraction (BV/TV), trabecular number (Tb.N), trabecular separation (Tb.Sp), and trabecular thickness (Tb.Th) were analyzed using systematic software, ensuring consistency across all specimens.

2.22. Quantification and statistical analysis

Statistical analysis was performed using GraphPad Prism. Significant differences were determined by *t*-test or one-way ANOVA where appropriate (*$p < 0.05$; **$p < 0.01$).

3. Results

3.1. Characteristics of exosomes derived from serum

The examination of exosomes under transmission electron microscopy revealed their sizes to range from 120 to 150 nm (Fig. 1B and C). Furthermore, the positive expression of exosome-specific marker proteins, including CD63, CD81, and TSG101, confirmed the successful isolation of exosomes (Fig. 1D). To verify their endocytic capacity, PKH26-labeled exosomes were introduced into hBMSCs, and subsequent visualization under a fluorescence microscope, following nuclear staining with DAPI, confirmed the internalization of these labeled exosomes (Fig. 1E).

3.2. Determination of optimal exosome concentration

To ascertain the most suitable concentration of exosomes for subsequent experimentation, varying concentrations of normal-exosomes were administered to hBMSCs. The assessment of bone-promoting and lipid-inhibiting effects, through ARS and Oil Red O staining respectively, led to the selection of 10^{11} particles per 100 μl as the optimal concentration for *in vitro* studies (Fig. 1F). This concentration was adopted for all subsequent experiments.

3.3. Regulation of osteogenesis and lipogenesis in BMSCs by serum-derived exosomes: in vitro and in vivo studies

This study aimed to elucidate the distinct biological functions of normal and osteoporosis-derived exosomes on bone marrow mesenchymal stem cells (BMSCs). By exposing hBMSCs to these two types of exosomes, we observed that normal exosomes significantly enhanced the expression of osteogenic markers (Runx2, OPN, ALP) and suppressed lipogenic markers (CEBPα, PPARγ) at both the mRNA and protein levels. Conversely, osteoporotic exosomes exhibited opposite effects (Fig. 2A–C). Immunofluorescence analysis further confirmed this trend, showcasing increased ALP and decreased PPARγ expression with normal exosomes (Fig. 2D, F). Functional assays revealed that normal exosomes promoted calcification and reduced lipid accumulation in hBMSCs, whereas osteoporotic exosomes had the opposite effects (Fig. 1E, G).

To assess the *in vivo* relevance, we injected these exosomes into ovariectomized mice. Micro-CT scans demonstrated that normal exosomes mitigated bone loss induced by ovariectomy, whereas osteoporotic exosomes exacerbated it (Figs. S1A and B). Subsequent analysis of BMSCs from these mice showed that normal exosomes elevated global m6A methylation levels and osteogenic markers while downregulating lipogenic markers. In contrast, osteoporotic exosomes had a weaker impact on m6A methylation and osteogenic/lipogenic gene expression (Figs. S1C–F).

3.4. METTL3 derived from serum was a candidate mRNA for postmenopausal osteoporosis

METTL3, an m6A methyltransferase derived from serum exosomes, emerged as a promising candidate mRNA in the context of postmenopausal osteoporosis. To unravel the endogenous mRNA cargo within serum exosomes that modulate these biological processes, we employed next-generation RNA sequencing. Our analysis revealed a comprehensive landscape of 1435 differentially expressed mRNAs (Fig. 3A and B), hinting at their potential involvement.

Notably, the m6A methylation status of bone marrow mesenchymal stem cells (hBMSCs) isolated from osteoporotic patients was conspicuously diminished compared to those from individuals with normal bone density (Fig. 3C). This finding led us to hypothesize that the assimilation of serum exosomes by hBMSCs might regulate osteogenic and adipogenic differentiation pathways through modulating the m6A methylation of pertinent genes.

To delve deeper into the underlying mechanism, we performed an intersectional analysis between the differentially expressed mRNAs and a curated list of m6A methylation-associated genes, including METTL3, METTL14, WTAP, ALKBH5, FTO, and YTHDF family members (YTHDF1, YTHDF2, YTHDF3, YTHDC1, YTHDC2) [17,18]. This comprehensive approach pinpointed METTL3 as a prime candidate gene of interest (Fig. 3D).

Subsequently, we quantitatively assessed the mRNA levels of METTL3 in serum exosomes harvested from 19 subjects with normal bone density and an equal number of osteoporotic patients using RT-qPCR. Intriguingly, normal serum exosomes exhibited significantly higher METTL3 mRNA expression (Fig. 3E). Furthermore, when these purified serum exosomes were introduced into hBMSCs, a notable alteration in METTL3 mRNA expression was observed (Fig. 3F), underscoring the dynamic interaction between serum exosomes and hBMSCs.

Collectively, our findings underscore the pivotal role of METTL3 within serum exosomes in orchestrating osteogenic and adipogenic differentiation in hBMSCs, thereby shedding light on potential therapeutic avenues for postmenopausal osteoporosis.

3.5. METTL3 promoted osteogenesis and reduced lipogenesis in hBMSCs

To rigorously validate the functional significance of METTL3 in hBMSCs, we manipulated its expression levels through knockdown and overexpression experiments. Our findings revealed a clear dichotomy in the expression patterns of osteogenic and lipogenic genes upon altering METTL3 levels. Specifically, METTL3 knockdown led to a downregulation of osteogenic markers (mRNA and protein) and a concurrent upregulation of lipogenic markers. Conversely, METTL3 overexpression resulted in an upregulation of osteogenic genes and a downregulation of lipogenic genes (Fig. 4A, B, C).

Immunofluorescence analysis further corroborated these results, demonstrating a decrease in Runx2 fluorescence intensity and an increase in PPARγ fluorescence upon METTL3 knockdown. Conversely,

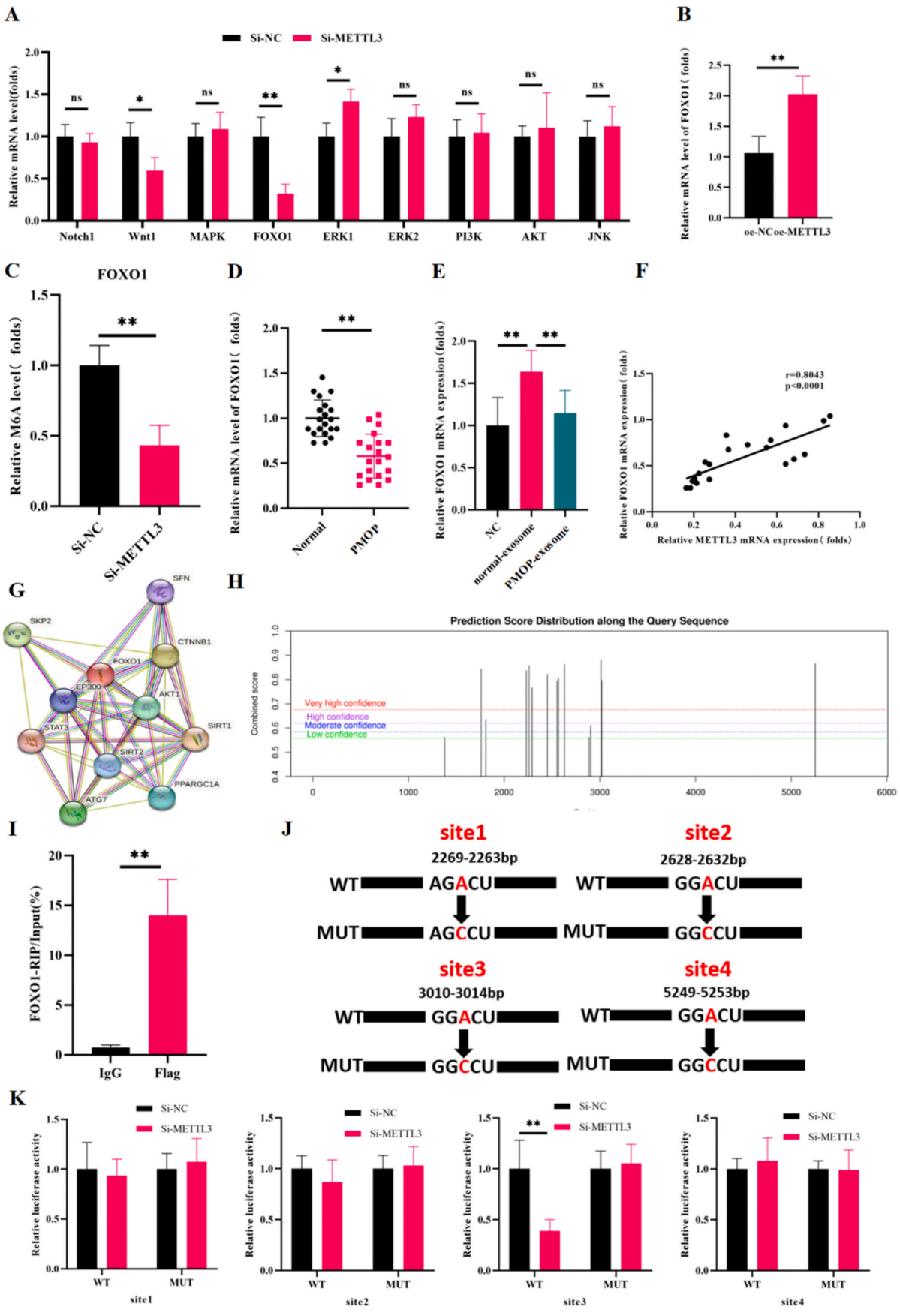

(caption on next page)

Fig. 5. METTL3 promotes m6A methylation of FOXO1. (A) qPCR analysis of Notch1, Wnt1, MAPK, FOXO1, ERK1, ERK2, PI3K, AKT, JNK mRNA expression transfected by si-METTL3 (n = 3). (B) qPCR analysis of FOXO1 mRNA expression transfected by METTL3 overexpression plasmid (n = 3). (C) m6A methylation level of FOXO1 after transfected by si-METTL3 (n = 3). (D) qPCR analysis of FOXO1 mRNA expression in human samples (19/19). (E) qPCR analysis of FOXO1 mRNA expression in hBMSCs treated with normal-exosome and PMOP-exosome. (F) The relationship between METTL3 and FOXO1 was assessed by Pearson correlation coefficient. (G) FOXO1 related proteins were predicted using the STRING online tool. (H) m6(A) methylation sites of FOXO1 were predicted using the SRAMP database. (I) The combination between METTL3 and FOXO1 was analyzed using RIP assay. (J) The potential bindings sites in FOXO1 were shown. (K) The luciferase reporter analysis evaluated which site of FOXO1 could be bound to METTL3. P values were calculated using Student's t-test. Data are expressed as the mean ± SD, *<0.05, **<0.01.

METTL3 overexpression enhanced Runx2 fluorescence and slightly diminished PPARγ fluorescence (Fig. 4D and E).

To visually assess the osteogenic and adipogenic potential of hBMSCs following METTL3 manipulation, we performed Alizarin Red S and Oil Red O staining. Notably, METTL3 knockdown was associated with a reduction in calcified nodules and an increase in lipid droplets, indicative of impaired osteogenesis and enhanced adipogenesis, respectively. In contrast, METTL3 overexpression led to an increase in calcified nodules and a decrease in lipid droplets, suggesting enhanced osteogenic differentiation and suppressed adipogenesis (Fig. 4F and G).

Collectively, these comprehensive results underscore the pivotal role of METTL3 in promoting osteogenic differentiation and inhibiting lipogenic differentiation in hBMSCs, thereby reinforcing its potential as a therapeutic target for bone-related disorders.

3.6. METTL3 affects osteogenesis and lipogenesis of hBMSCs by regulating m6A methylation of FOXO1

To unravel the molecular mechanisms underlying METTL3's influence on osteogenesis and lipogenesis in hBMSCs, we delved into its downstream regulatory network [19–25]. Following METTL3 knockdown and overexpression, qPCR analysis revealed a significant downregulation of FOXO1 expression upon METTL3 suppression and upregulation upon its overexpression (Fig. 5A and B). Utilizing MeRIP-PCR, we observed a reduction in m6A methylation levels of FOXO1 mRNA upon METTL3 knockdown, suggesting METTL3's role in modulating FOXO1's m6A status (Fig. 5C).

Further validation in patient-derived BMSCs confirmed that FOXO1 mRNA expression was elevated in individuals with normal bone mineral density (BMD), both intrinsically (Fig. 5D) and exogenously through serum exosome treatment (Fig. 5E). Based on these findings, we hypothesized FOXO1 as a potential downstream effector of METTL3.

To strengthen this connection, we analyzed the correlation between METTL3 and FOXO1 mRNA expression in BMSCs from osteoporosis patients, revealing a robust positive correlation ($r = 0.8043$, $P < 0.0001$) (Fig. 5F). To gain insights into FOXO1's functional interactions, we explored its Protein-Protein Interaction (PPI) networks using the STRING database (Fig. 5G).

To directly demonstrate METTL3's interaction with FOXO1 mRNA, we performed RNA Immunoprecipitation (RIP) experiments, confirming METTL3's ability to bind FOXO1 mRNA (Fig. 5I). To pinpoint the specific m6A methylation sites on FOXO1 mRNA targeted by METTL3, we predicted and screened candidate sites using the SRAMP database, focusing on the four highest-scoring sites (>0.850) (Fig. S4). Luciferase Reporter Assays subsequently identified site 3 (3012bp) as the key m6A methylation binding site (Fig. 5H, J, K).

These findings collectively establish METTL3 as a critical regulator of FOXO1 m6A methylation, thereby modulating osteogenesis and lipogenesis in hBMSCs, with implications for bone health and disease.

3.7. FOXO1 promoted osteogenesis and reduced lipogenesis in hBMSCs

FOXO1 emerged as a pivotal regulator enhancing osteogenesis while suppressing lipogenesis in human bone marrow mesenchymal stem cells (hBMSCs). To substantiate this role, we manipulated FOXO1 expression levels in hBMSCs and assessed their impact on osteogenic and lipogenic pathways. Our findings revealed that FOXO1 knockdown led to a pronounced downregulation of osteogenic-related gene expression at both mRNA and protein levels, accompanied by an upregulation of lipogenic gene markers (Fig. 6A, B, C). Conversely, FOXO1 overexpression augmented osteogenic differentiation while attenuating lipogenic differentiation, as evidenced by the reciprocal expression patterns of respective gene sets.

Immunofluorescence analysis further corroborated these results, demonstrating a decrease in Runx2 (a key osteogenic marker) fluorescence intensity and an increase in PPARγ (a lipogenic transcription factor) fluorescence following FOXO1 knockdown. Conversely, FOXO1 overexpression enhanced Runx2 fluorescence and modestly reduced PPARγ fluorescence (Fig. 6D, F).

Histochemical staining with Alizarin Red and Oil Red O provided visual confirmation of these molecular changes. Specifically, FOXO1 knockdown resulted in fewer calcium nodules (indicative of osteogenic differentiation) and increased lipid droplets (indicative of lipogenic differentiation) in hBMSCs, whereas FOXO1 overexpression yielded the opposite effect, characterized by more calcium nodules and fewer lipid droplets (Fig. 6E, G).

Collectively, these results underscore FOXO1's dual function in promoting osteogenic differentiation and inhibiting lipogenic differentiation in hBMSCs, underscoring its potential as a therapeutic target for modulating bone health and metabolism.

3.8. METTL3 promoted osteogenesis and inhibited lipogenesis of hBMSCs by regulating FOXO1 mRNA expression

To elucidate the mechanism underlying METTL3's influence on osteogenesis and lipogenesis in human bone marrow mesenchymal stem cells (hBMSCs) through modulation of FOXO1 mRNA expression, we conducted a series of experiments. Specifically, we overexpressed the METTL3 gene in hBMSCs and subsequently downregulated FOXO1 expression. Our results demonstrated that METTL3 overexpression led to a significant upregulation of osteogenic-related mRNA and protein markers, which was reversed upon FOXO1 knockdown (Fig. 7A, B, C). Conversely, METTL3 overexpression suppressed lipogenic-related mRNA and protein markers, with this inhibition being mitigated by FOXO1 downregulation.

Immunofluorescence analysis, Alizarin Red staining for osteogenic differentiation, and Oil Red O staining for lipogenic differentiation further validated these findings. Specifically, METTL3 overexpression enhanced osteogenic markers while diminishing lipogenic markers, whereas FOXO1 knockdown attenuated the osteogenic effects and exacerbated the lipogenic effects induced by METTL3 overexpression (Fig. 7D, E, F, G).

Collectively, these results provide compelling evidence that METTL3 promotes osteogenesis and inhibits lipogenesis in hBMSCs by positively regulating FOXO1 mRNA expression, thereby highlighting the intricate interplay between epigenetic regulators and transcription factors in governing bone metabolism and adipogenesis.

Drawing from the aforementioned experimental outcomes, we conclusively determined that METTL3, through its role in m6A methylation, fosters the expression of FOXO1 mRNA, thereby augmenting osteogenesis and concurrently suppressing lipogenesis in human bone marrow mesenchymal stem cells (hBMSCs). This finding underscores the pivotal role of METTL3 in fine-tuning the balance between bone formation and fat accumulation in these critical progenitor

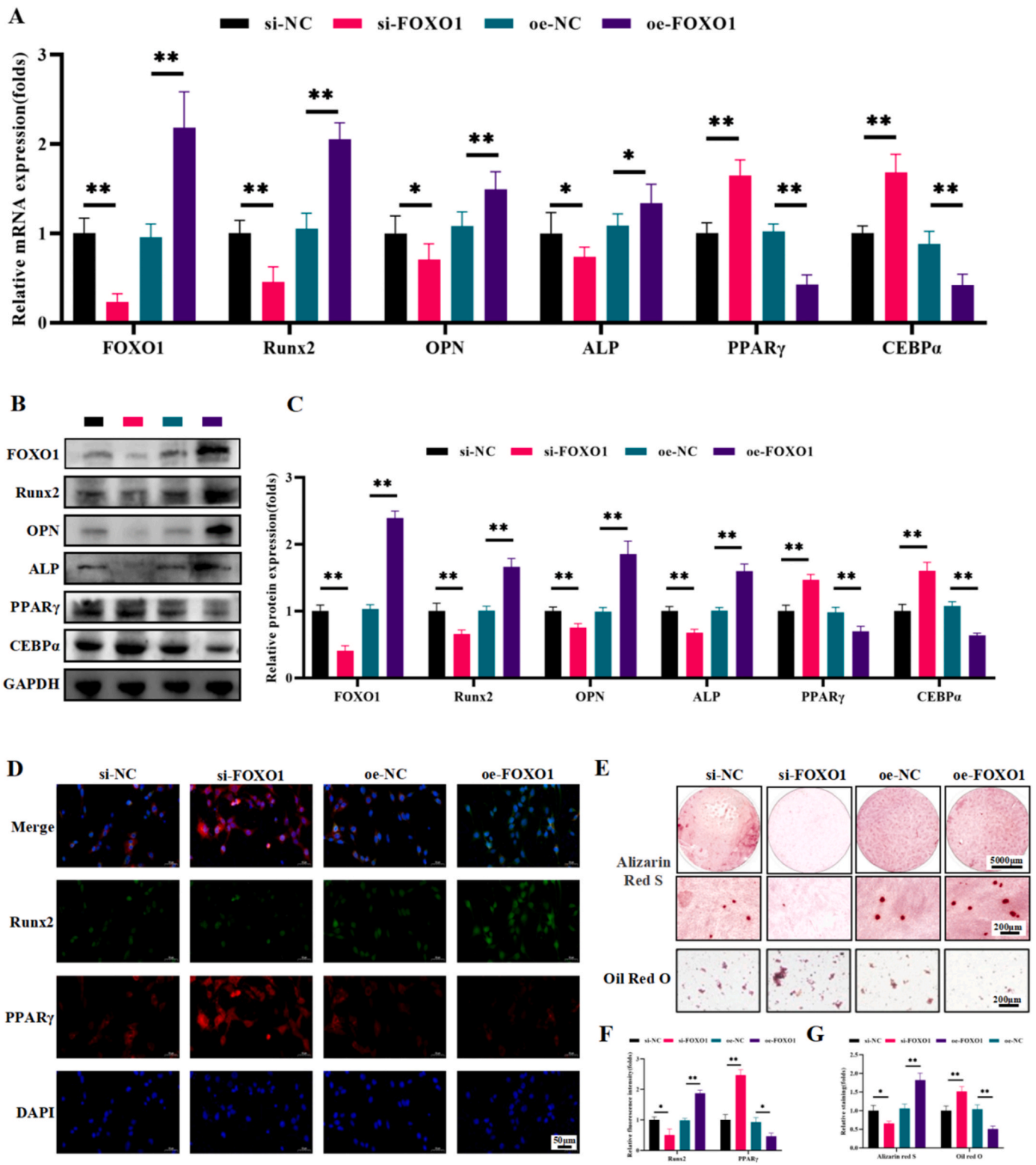

Fig. 6. FOXO1 promotes osteogenesis and inhibits lipogenesis in hBMSCs. (A) qPCR analysis of FOXO1, Runx2, OPN, ALP, PPARγ, CEBPα mRNA expression transfected by si-FOXO1 and FOXO1 overexpression plasmid (n = 3). (B) Western blot analysis of FOXO1, osteogenesis and lipogenesis-related markers. (C) Quantification analysis of FOXO1, osteogenesis and lipogenesis-related protein expression (n = 3). (D) Immunofluorescence of Runx2 and PPARγ in hBMSCs transfected by si-FOXO1 and FOXO1 overexpression plasmid. (E) Alizarin red S staining and Oli red O staining. (F) Quantification analysis of immunofluorescence of Runx2 and PPARγ(n = 3). (G) Quantification analysis of Alizarin red S staining and oli red O staining (n = 3). P values were calculated using Student's t-test. Data are expressed as the mean ± SD, *<0.05, **<0.01.

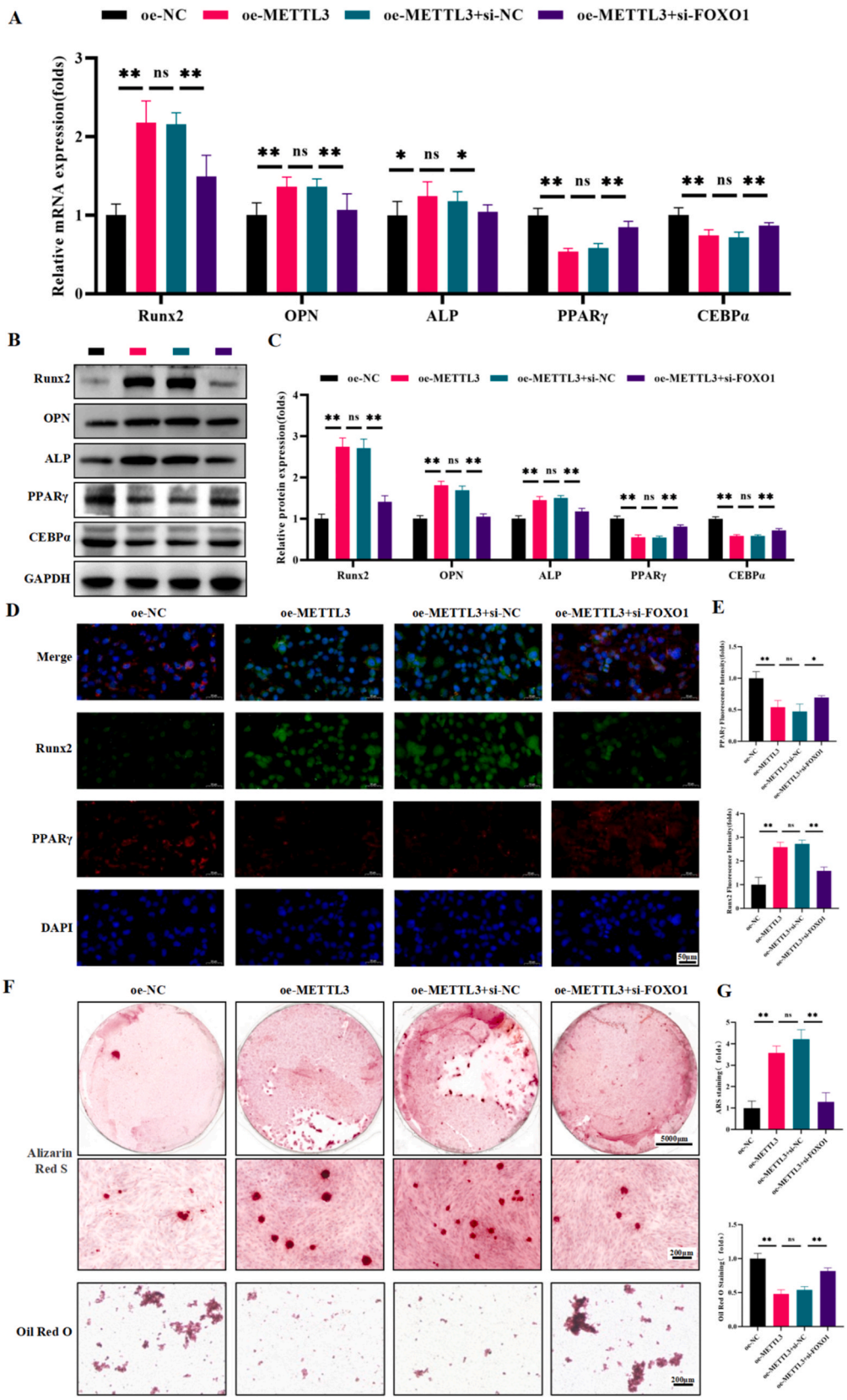

Fig. 7. Knocking down FOXO1 can block the osteogenic and lipogenic effects of METTL3 in hBMSCs. (A) qPCR analysis of osteogenesis and lipogenesis related mRNA expression (n = 3). (B) Western blot analysis of osteogenesis and lipogenesis-related markers. (C) Quantification analysis of osteogenesis and lipogenesis-related protein expression (n = 3). (D) Immunofluorescence of Runx2 and PPARγ in hBMSCs transfected by si-FOXO1 and FOXO1 overexpression plasmid. (E) Quantification analysis of immunofluorescence of Runx2 and PPARγ(n = 3). (F) Alizarin red S staining and Oli red O staining. (G) Quantification analysis of Alizarin red S staining and oli red O staining (n = 3). P values were calculated using Student's t-test. Data are expressed as the mean ± SD, *<0.05, **<0.01.

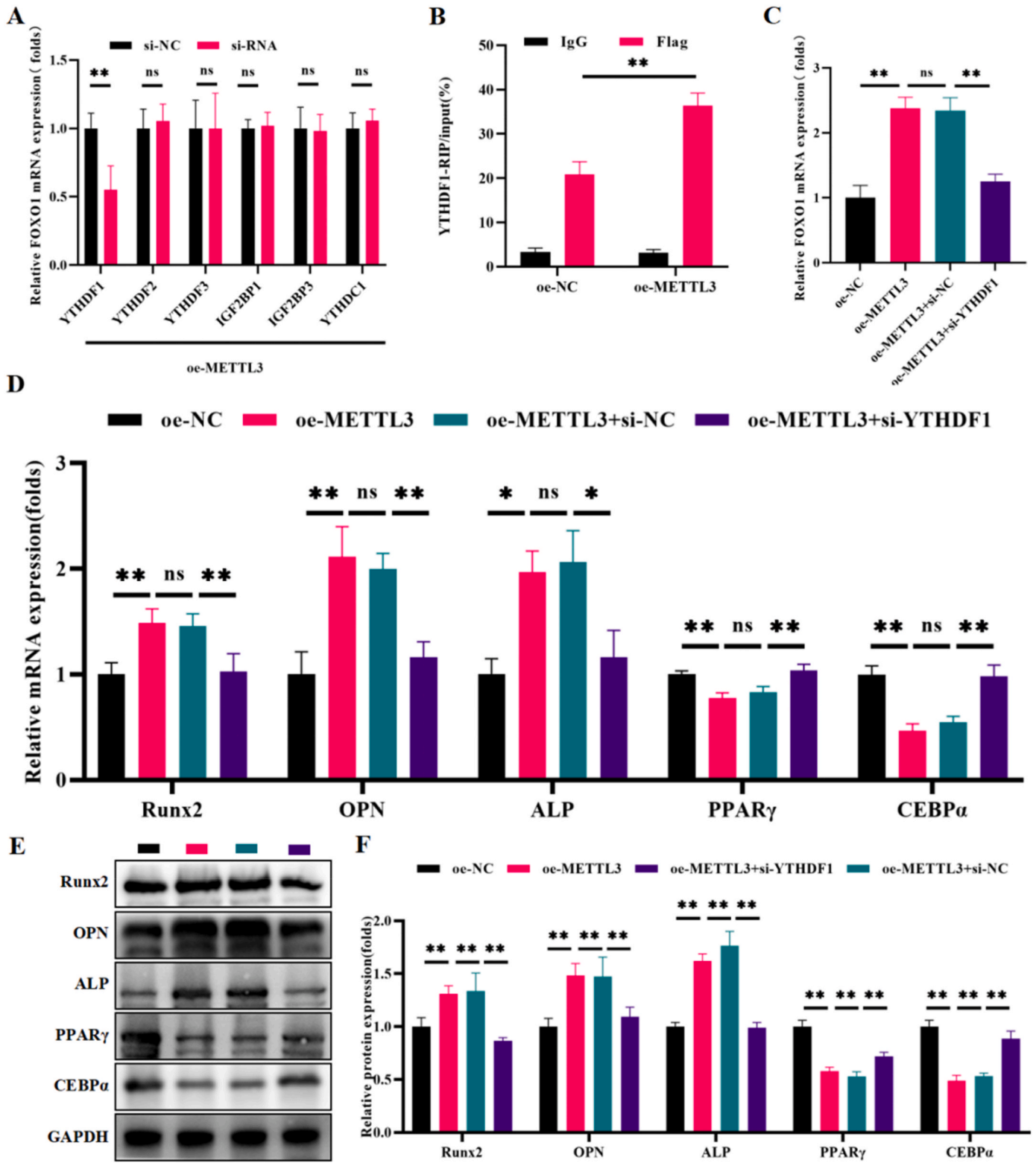

Fig. 8. METTL3 positively regulates FOXO1 in a YTHDF1 manner. (A) qPCR analysis of YTHDF1, YTHDF2, YTHDF3, IGF2BP1, IGF2BP3, YTHDC1 mRNA expression after transfection (n = 3). (B) The combination between YTHDF1 and FOXO1 was analyzed using RIP assay. (C) qPCR analysis of FOXO1 mRNA expression (n = 3). (D) qPCR analysis of osteogenesis and lipogenesis related mRNA expression (n = 3). (E) Western blot analysis of osteogenesis and lipogenesis-related markers. (F) Quantification analysis of osteogenesis and lipogenesis-related protein expression (n = 3). P values were calculated using Student's t-test. Data are expressed as the mean ± SD, *<0.05, **<0.01.

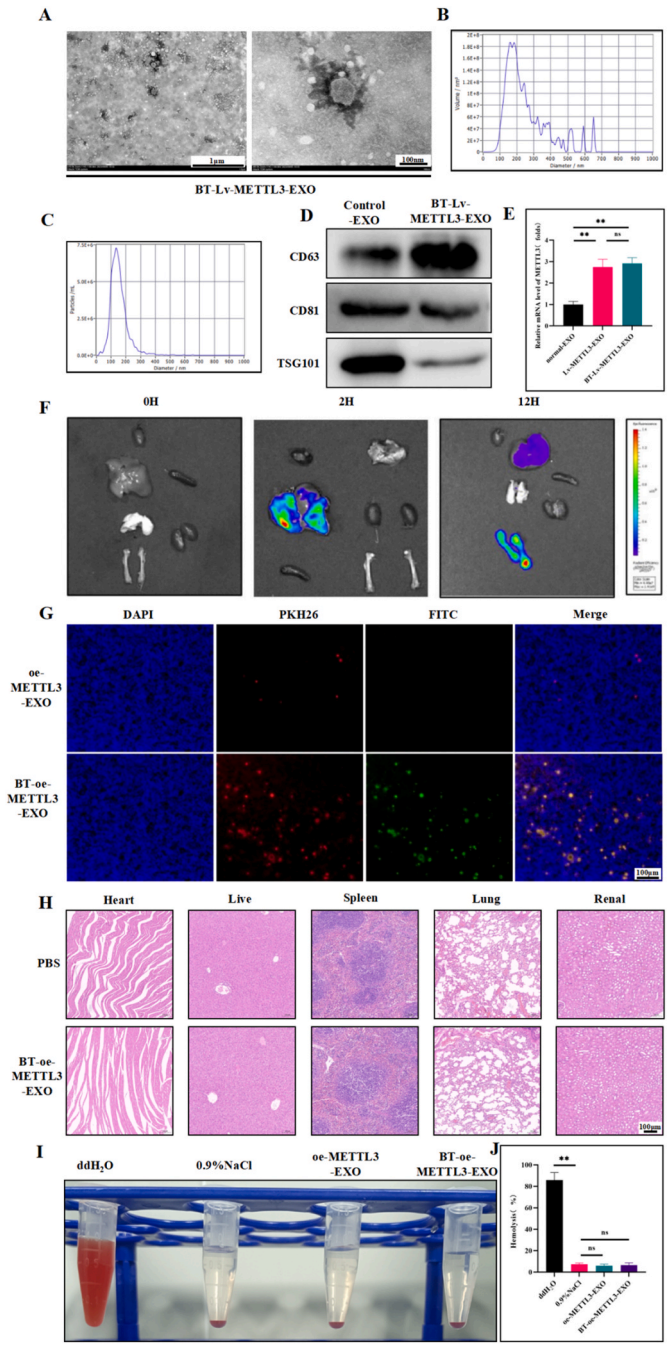

Fig. 9. Synthesis and bone targeting properties of BT-oe-METTL3-EXO. (A) TEM images of BT-oe-METTL3-EXO. (B–C) NTA analysis of BT-oe-METTL3-EXO. (D) Western blot analysis of exosome-specific markers, CD63, CD81 and TSG101. (E) qPCR analysis of METTL3 mRNA expression (n = 3). (F) Fluorescence of organs from mice sacrificed 0 h, 2 h, 12 h after intravenous injection of BT-oe-METTL3-EXO. (G) Fluorescence of femur from mice after intravenous injection of BT-oe-METTL3-EXO.Exosome was labeled with PKH26, bone target peptide was labeled with FITC. (H) HE staining of organs from mice after intravenous injection of BT-oe-METTL3-EXO.(I) The biocompatibility of various exosomes was verified by hemolysis test. (I) Quantification of hemolysis rate of 4 kinds of solutions. P values were calculated using Student's t-test. Data are expressed as the mean ± SD, *<0.05, **<0.01.

cells, revealing a novel epigenetic regulatory axis that governs the lineage commitment of hBMSCs.

3.9. METTL3-mediated m6A modification increased the FOXO1 mRNA level in a YTHDF1-dependent manner

We uncovered that METTL3-mediated m6A modification enhances FOXO1 mRNA levels in a YTHDF1-specific manner. To pinpoint the reader protein involved in the m6A methylation of FOXO1 mRNA, we conducted a systematic knockdown of known m6A reader genes, namely YTHDF1, YTHDF2, YTHDF3, IGF2BP1, IGF2BP3, and YTHDC1 [26–31], and assessed FOXO1 mRNA expression via RT-PCR (Fig. 8A). Notably, the ablation of YTHDF1 attenuated the METTL3-induced upregulation of FOXO1 mRNA in hBMSCs (Fig. 8C). This observation was corroborated by YTHDF1-RIP analysis, which demonstrated that METTL3 overexpression significantly enhanced m6A modification of FOXO1 mRNA, an effect that was contingent upon YTHDF1 (Fig. 8B).

Furthermore, we found that YTHDF1 knockdown mitigated the osteogenic stimulation and alleviated the lipogenic repression mediated by METTL3 overexpression, as evidenced by functional assays (Fig. 8D, E, F). Collectively, our data convincingly demonstrate that METTL3-driven m6A modification elevates FOXO1 expression in a manner that is critically dependent on YTHDF1, elucidating a novel regulatory axis that integrates epigenetic modifications with post-transcriptional processing to modulate the fate of hBMSCs.

3.10. Development and bone-targeting capability of BT-oe-METTL3-EXO

To achieve precise and potent modulation of osteogenesis enhancement and lipogenesis suppression in bone marrow stromal cells (BMSCs), our research group engineered an exosome equipped with bone-targeting capabilities. Transmission electron microscopy and nanoparticle tracking analysis (NTA) validated the successful isolation of exosomes with a uniform diameter of approximately 135 nm, and confirmed the presence of characteristic surface marker proteins (Fig. 9A, B, C, and D). Quantitative RT-PCR analysis revealed a marked upregulation of METTL3 mRNA within these engineered exosomes (Fig. 9E), indicating successful genetic modification.

Biophotonic imaging conducted 12 h post-tail vein injection in mice demonstrated a significant accumulation of exosomes within the femur (Fig. 9F). Fluorescence microscopy of femur sections further corroborated the superior bone-targeting efficiency of our engineered exosomes compared to non-targeted counterparts, exhibiting a heightened enrichment within the bone tissue (Fig. 9G). Additionally, histological examination of mouse viscera following HE staining confirmed the excellent biocompatibility of these bone-targeting exosomes, with no apparent toxicity or adverse effects (Fig. 9H).At the same time, the hemolytic test confirmed that the bone-targeting exosome we synthesized did not have obvious toxicity to red blood cells (Fig. 9I and J).

This comprehensive evaluation underscores the potential of BT-oe-METTL3-EXO as a promising therapeutic vector for targeted modulation of bone metabolism, offering a novel and safe approach for the treatment of bone-related disorders.

3.11. Promotion of osteogenic differentiation and inhibition of lipogenic differentiation in ovariectomized mice by BT-oe-METTL3-EXO

To elucidate the anabolic potential of BT-oe-METTL3-EXO *in vivo*, we administered oe-METTL3-EXO, BT-oe-METTL3-EXO, or PBS to ovariectomized (OVX) mice and sham-operated controls over a 6-week period, with injections every two days (Fig. 10A). Micro-computed tomography (μCT) analysis unveiled that both oe-METTL3-EXO and BT-oe-METTL3-EXO effectively countered OVX-induced bone loss. However, the bone mass-preserving effect of BT-oe-METTL3-EXO was notably more pronounced than that of oe-METTL3-EXO (Fig. 10B and C).

Histological assessment of tibia sections through hematoxylin and

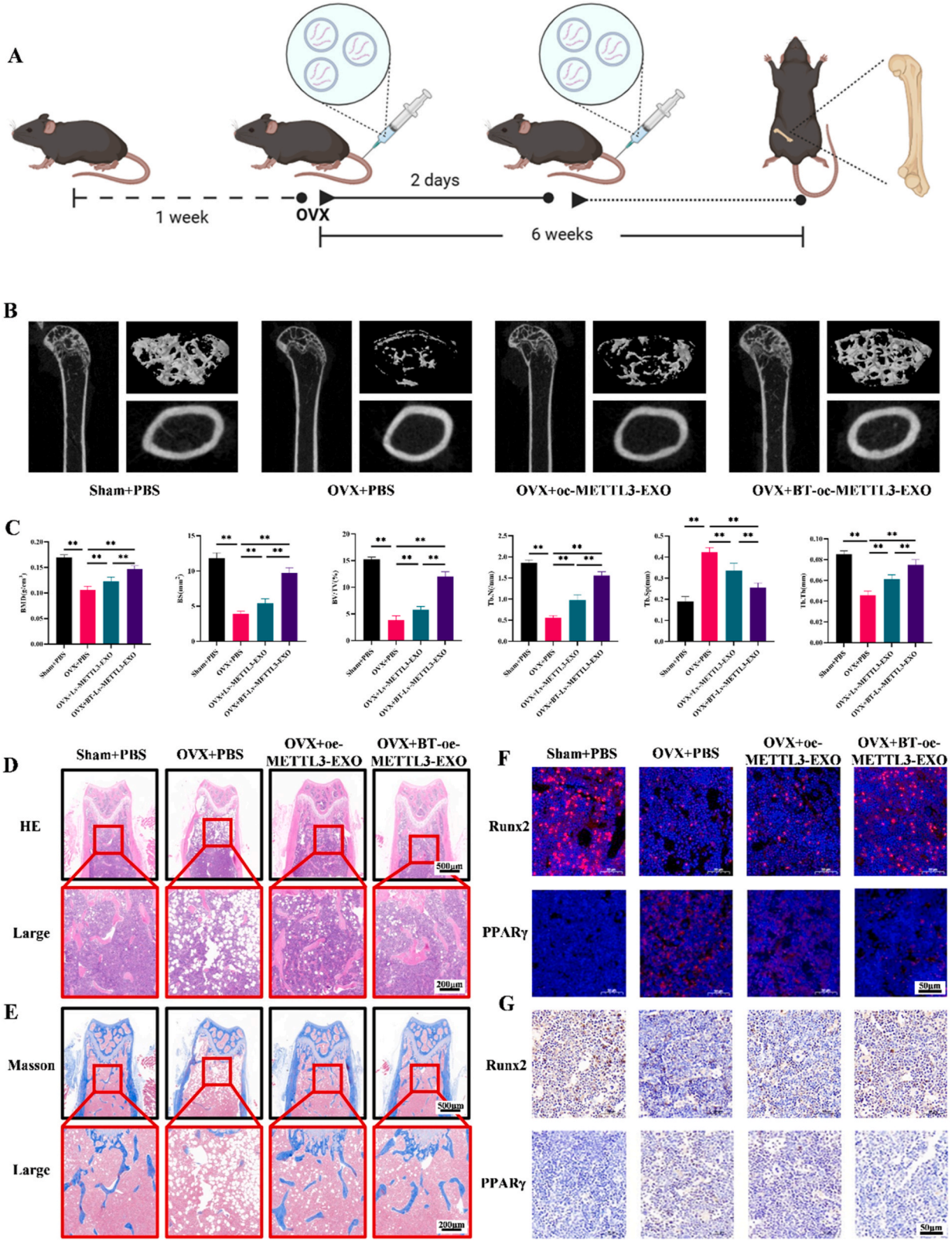

Fig. 10. Validation of the function of BT-oe-METTL3-EXO *in vitro*. (A) Illustration of experimental protocols for the creation of osteoporosis mice by ovariectomy and administration of PBS, oe-METTL3-EXO or BT-oe-METTL3-EXO to OVX mice and sham-operated control counterparts. (B) Micro-CT image of distal (C) Quantification analysis of BMD, BT/TV, BS. Tb.N, Tb. Sp, Tb.Th in distal femur of mice (n = 6). (D–E) Representative images of H&E and Masson staining of mice femurs showing the ameliorating effects of BT-oe-METTL3-EXO on the reduction of bone formation in OVX mice. (F) Representative images of immunofluorescence staining (G) Representative images of immunohistochemical staining. (E) Western blot analysis of osteogenesis and lipogenesis-related markers. (F) Quantification analysis of osteogenesis and lipogenesis-related protein expression. P values were calculated using Student's t-test. Data are expressed as the mean ± SD, *<0.05, **<0.01.

eosin (H&E) staining and Masson's trichrome staining further substantiated the μCT findings, revealing a superior increase in trabecular bone density in mice treated with BT-oe-METTL3-EXO (Fig. 10D and E). Immunofluorescence and immunohistochemical analysis of femur sections indicated a heightened presence of alkaline phosphatase (ALP)-positive cells, indicative of osteogenic activity, and a decrease in peroxisome proliferator-activated receptor gamma (PPARγ)-positive cells, suggesting reduced adipogenesis in mice injected with BT-oe-METTL3-EXO (Fig. 10F and G).

Concomitantly, the expression levels of osteogenic-related genes were significantly upregulated at both the mRNA and protein levels in mice treated with BT-oe-METTL3-EXO, whereas the expression of lipogenic genes was downregulated (Figure S4A,B and C). These findings collectively underscore the dual therapeutic potential of BT-oe-METTL3-EXO in promoting osteogenic differentiation and inhibiting lipogenic differentiation in ovariectomized mice. Simultaneously, akin to *in vitro* experiments, the caudal intravenous injection of substances oe-METTL3-EXO and BT-oe-METTL3-EXO elevated the mRNA and protein expression of METTL3 and FOXO1 in mouse bone marrow mesenchymal stem cells, as well as the m6A levels. However, the effect of BT-oe-METTL3-EXO was markedly superior to that of oe-METTL3-EXO. Furthermore, the introduction of oe-METTL3-EXO and BT-oe-METTL3-EXO *in vivo* did not influence the mRNA and protein expression of YTHDF1 (Figs. S4D,E, F, and G). The results suggest that the expression of YTHDF1 remains unaffected by alterations in METTL3 expression. Our *in vitro* experiments confirmed that BT-oe-METTL3-EXO at a concentration of 10^{11}/100 μl can perform the same functions as E2 at a concentration of 10^{-8} M in promoting bone differentiation and inhibiting lipid differentiation (Figure S5A,B and C).

4. Discussion

Osteoporosis, a metabolic bone ailment marked by diminished bone mass and adipose tissue accumulation within the bone marrow, poses a burgeoning public health challenge [1,32]. Recent research underscores the pivotal role of exosomes in the onset and progression of this condition [33–35]. Notably, as osteoporosis is systemic, alterations in serum exosomes hold significant implications for its development [36–38]. Our *in vitro* investigations revealed that normal-exosomes (derived from individuals with normal bone mineral density) promoted osteogenesis and markedly suppressed lipogenesis in human bone marrow stromal cells (hBMSCs). Furthermore, these normal-exosomes mitigated bone loss in ovariectomized mice.

To delve deeper into the underlying mechanisms, we performed mRNA sequencing on two types of exosomes, identifying 1435 differentially expressed mRNAs. Building upon prior research indicating low m6A methylation levels in BMSCs of osteoporosis patients [14,39,40], we screened for m6A methylation-associated genes among these differentially expressed transcripts. Strikingly, METTL3 expression emerged as a notable difference. *In vitro* assays confirmed that METTL3 positively correlated with osteogenesis and inversely with lipogenesis in hBMSCs.

FOXO1, a member of the FOXOs protein family, has been shown to collaborate with RUNX2, enhancing the expression of osteogenic markers like RUNX2, ALP, and OPN, while inhibiting PPARγ [41–43]. In our study, FOXO1 expression was diminished in hBMSCs from osteoporosis patients but augmented upon treatment with normal-exosomes. Knockdown of FOXO1 reduced osteogenesis and exacerbated lipogenesis in hBMSCs. Through RIP experiments, we discovered that METTL3 exerts its biological function by binding to FOXO1 mRNA at a specific site (GGACU), modulating its m6A methylation. Additionally, reader proteins, essential components of the m6A methylation machinery, enhance mRNA translation efficiency, stabilize transcripts, and regulate selective cleavage [44–48]. Our findings indicated that YTHFD1 binds to FOXO1, accelerating its translation.

mRNA, as the primary conveyor of genetic information, offers several inherent advantages in therapeutic applications. Firstly, mRNA introduction avoids reverse transcriptase, thus preventing genomic integration and DNA alterations. Secondly, erroneous mRNA therapy, though potentially yielding side effects, is time-limited and non-integrative, allowing reversibility upon treatment cessation. However, mRNA's structural similarity to viruses and bacteria prompts innate immune recognition, potentially triggering inflammatory responses and impeding its intended function [49,50]. Our study elegantly circumvents this hurdle by harnessing exosomes as mRNA delivery vehicles. Moreover, to enhance exosome efficacy and mitigate side effects, we incorporated bone-targeting peptides onto their surface. Animal models demonstrated that these modified exosomes accumulated preferentially in bone tissue, exhibiting superior bone loss mitigation, osteogenesis promotion, and lipogenesis suppression in BMSCs compared to their unmodified counterparts.

5. Conclusion

This study delves into the intricate mechanisms of serum exosomes, uncovering their pivotal role in modulating the onset and progression of postmenopausal osteoporosis. By pinpointing potential mRNA targets, we have successfully engineered exosomes as a targeted therapeutic mRNA delivery system. These engineered exosomes demonstrate remarkable efficacy in mitigating bone loss induced by ovariectomy in mice models, while also mitigating side effects, thereby presenting substantial promise for clinical translation in the treatment of postmenopausal osteoporosis.

6. Limitations

Notably, our investigation has its boundaries. Firstly, we have yet to explore the specific functions of METTL3 and FOXO1 within osteoclasts, which could provide further insights into the regulatory landscape of bone metabolism. Secondly, the versatility of our engineered therapeutic exosomes remains to be validated in diverse osteoporosis models, expanding their potential applications beyond postmenopausal cases.

CRediT authorship contribution statement

Tao Li: Writing – original draft, Methodology, Investigation, Conceptualization. **Jiangminghao Zhao:** Validation, Methodology, Data curation. **Jinghong Yuan:** Visualization, Formal analysis. **Rui Ding:** Visualization, Formal analysis. **Guoyu Yang:** Software, Resources. **Jian Cao:** Software, Resources. **Xiaokun Zhao:** Validation. **Jiahao Liu:** Validation. **Yuan Liu:** Formal analysis. **Peichuan Xu:** Formal analysis. **Jianjian Deng:** Supervision, Project administration. **Xinxin Miao:** Supervision, Project administration. **Xigao Cheng:** Project administration, Funding acquisition, Conceptualization.

Declaration of competing interest

The authors declare that there are no conflict of interests, we do not have any possible conflicts of interest.

Acknowledgments

National Natural Science Foundation of China (82060403, 81860397), Double Thousand Plan of Jiangxi Province (JXSQ2019201026).

Appendix A. Supplementary data

Supplementary data to this article can be found online at https://doi.org/10.1016/j.mtbio.2025.101648.

Data availability

Data will be made available on request.

References

[1] L. Wang, W. Yu, X. Yin, L. Cui, S. Tang, N. Jiang, et al., Prevalence of osteoporosis and fracture in China: the China osteoporosis prevalence study, JAMA Netw. Open 4 (8) (2021) e2121106.

[2] S. Khandelwal, N.E. Lane, Osteoporosis: review of etiology, mechanisms, and approach to management in the aging population, Endocrinol Metab. Clin. N. Am. 52 (2) (2023) 259–275.

[3] V. Gopinath, Osteoporosis, Med. Clin. North Am. 107 (2) (2023) 213–225.

[4] E.M. Curtis, R.J. Moon, N.C. Harvey, C. Cooper, The impact of fragility fracture and approaches to osteoporosis risk assessment worldwide, Bone 104 (2017) 29–38.

[5] F.R. Pérez-López, Postmenopausal osteoporosis and alendronate, Maturitas 48 (3) (2004) 179–192.

[6] H.G. Bone, R.B. Wagman, M.L. Brandi, J.P. Brown, R. Chapurlat, S.R. Cummings, et al., 10 years of denosumab treatment in postmenopausal women with osteoporosis: results from the phase 3 randomised FREEDOM trial and open-label extension, Lancet Diabetes Endocrinol. 5 (7) (2017) 513–523.

[7] D.L. Kendler, F. Marin, C.A.F. Zerbini, L.A. Russo, S.L. Greenspan, V. Zikan, et al., Effects of teriparatide and risedronate on new fractures in post-menopausal women with severe osteoporosis (VERO): a multicentre, double-blind, double-dummy, randomised controlled trial, Lancet 391 (10117) (2018) 230–240.

[8] R. Narayanan, C.-C. Huang, S. Ravindran, Hijacking the cellular mail: exosome mediated differentiation of mesenchymal stem cells, Stem Cell. Int. 2016 (2016) 3808674.

[9] Y. Qin, L. Wang, Z. Gao, G. Chen, C. Zhang, Bone marrow stromal/stem cell-derived extracellular vesicles regulate osteoblast activity and differentiation *in vitro* and promote bone regeneration *in vivo*, Sci. Rep. 6 (2016) 21961.

[10] Y. Liang, L. Duan, J. Lu, J. Xia, Engineering exosomes for targeted drug delivery, Theranostics 11 (7) (2021) 3183–3195.

[11] H.P. Bei, P.M. Hung, H.L. Yeung, S. Wang, X. Zhao, Bone-a-Petite: engineering exosomes towards bone, osteochondral, and cartilage repair, Small 17 (50) (2021) e2101741.

[12] Y. Cui, Y. Guo, L. Kong, J. Shi, P. Liu, R. Li, et al., A bone-targeted engineered exosome platform delivering siRNA to treat osteoporosis, Bioact. Mater. 10 (2022) 207–221.

[13] Y. Hu, X. Li, Q. Zhang, Z. Gu, Y. Luo, J. Guo, et al., Exosome-guided bone targeted delivery of Antagomir-188 as an anabolic therapy for bone loss, Bioact. Mater. 6 (9) (2021) 2905–2913.

[14] Y. Wu, L. Xie, M. Wang, Q. Xiong, Y. Guo, Y. Liang, et al., Mettl3-mediated m6A RNA methylation regulates the fate of bone marrow mesenchymal stem cells and osteoporosis, Nat. Commun. 9 (1) (2018) 4772.

[15] Q. Zhang, R.C. Riddle, Q. Yang, C.R. Rosen, D.C. Guttridge, N. Dirckx, et al., The RNA demethylase FTO is required for maintenance of bone mass and functions to protect osteoblasts from genotoxic damage, Proc. Natl. Acad. Sci. U. S. A 116 (36) (2019) 17980–17989.

[16] M. He, H. Lei, X. He, Y. Liu, A. Wang, Z. Ren, et al., METTL14 regulates osteogenesis of bone marrow mesenchymal stem cells via inducing autophagy through m6A/IGF2BPs/beclin-1 signal Axis, Stem Cells Transl. Med. 11 (9) (2022).

[17] S. Oerum, V. Meynier, M. Catala, C. Tisné, A comprehensive review of m6A/m6Am RNA methyltransferase structures, Nucleic Acids Res. 49 (13) (2021) 7239–7255.

[18] Y. Li, L. Meng, B. Zhao, The roles of N6-methyladenosine methylation in the regulation of bone development, bone remodeling and osteoporosis, Pharmacol. Ther. 238 (2022) 108174.

[19] H. Han, H. Xiao, Z. Wu, L. Liu, M. Chen, H. Gu, et al., The miR-98-3p/JAG1/Notch1 axis mediates the multigenerational inheritance of osteopenia caused by maternal dexamethasone exposure in female rat offspring, Exp. Mol. Med. 54 (3) (2022) 298–308.

[20] C.M. Laine, K.S. Joeng, P.M. Campeau, R. Kiviranta, K. Tarkkonen, M. Grover, et al., WNT1 mutations in early-onset osteoporosis and osteogenesis imperfecta, N. Engl. J. Med. 368 (19) (2013) 1809–1816.

[21] L. Xiao, M. Zhong, Y. Huang, J. Zhu, W. Tang, D. Li, et al., Puerarin alleviates osteoporosis in the ovariectomy-induced mice by suppressing osteoclastogenesis via inhibition of TRAF6/ROS-dependent MAPK/NF-κB signaling pathways, Aging (Albany NY) 12 (21) (2020) 21706–21729.

[22] Y. Jiang, W. Luo, B. Wang, X. Wang, P. Gong, Y. Xiong, Resveratrol promotes osteogenesis via activating SIRT1/FoxO1 pathway in osteoporosis mice, Life Sci. 246 (2020) 117422.

[23] D. Fan, D. Fan, W. Yuan, CMTM3 suppresses bone formation and osteogenic differentiation of mesenchymal stem cells through inhibiting Erk1/2 and RUNX2 pathways, Genes Dis. 8 (6) (2021) 882–890.

[24] F. Zhao, Y. Xu, Y. Ouyang, Z. Wen, G. Zheng, T. Wan, et al., Silencing of miR-483-5p alleviates postmenopausal osteoporosis by targeting SATB2 and PI3K/AKT pathway, Aging (Albany NY) 13 (5) (2021) 6945–6956.

[25] X.-J. Li, Z. Zhu, S.-L. Han, Z.-L. Zhang, Bergapten exerts inhibitory effects on diabetes-related osteoporosis via the regulation of the PI3K/AKT, JNK/MAPK and NF-κB signaling pathways in osteoprotegerin knockout mice, Int. J. Mol. Med. 38 (6) (2016) 1661–1672.

[26] D. Han, J. Liu, C. Chen, L. Dong, Y. Liu, R. Chang, et al., Anti-tumour immunity controlled through mRNA m6A methylation and YTHDF1 in dendritic cells, Nature 566 (7743) (2019) 270–274.

[27] D. Dixit, B.C. Prager, R.C. Gimple, H.X. Poh, Y. Wang, Q. Wu, et al., The RNA m6A reader YTHDF2 maintains oncogene expression and is a targetable dependency in glioblastoma stem cells, Cancer Discov. 11 (2) (2021) 480–499.

[28] G. Chang, L. Shi, Y. Ye, H. Shi, L. Zeng, S. Tiwary, et al., YTHDF3 induces the translation of m6A-enriched gene transcripts to promote breast cancer brain metastasis, Cancer Cell 38 (6) (2020).

[29] S. Müller, M. Glaß, A.K. Singh, J. Haase, N. Bley, T. Fuchs, et al., IGF2BP1 promotes SRF-dependent transcription in cancer in a m6A- and miRNA-dependent manner, Nucleic Acids Res. 47 (1) (2019) 375–390.

[30] W. Wan, X. Ao, Q. Chen, Y. Yu, L. Ao, W. Xing, et al., METTL3/IGF2BP3 axis inhibits tumor immune surveillance by upregulating N6-methyladenosine modification of PD-L1 mRNA in breast cancer, Mol. Cancer 21 (1) (2022) 60.

[31] J. Liu, M. Gao, J. He, K. Wu, S. Lin, L. Jin, et al., The RNA m6A reader YTHDC1 silences retrotransposons and guards ES cell identity, Nature 591 (7849) (2021) 322–326.

[32] J.E. Compston, M.R. McClung, W.D. Leslie, Osteoporosis, Lancet 393 (10169) (2019) 364–376.

[33] D.-K. Kim, G. Bandara, Y.-E. Cho, H.D. Komarow, D.R. Donahue, B. Karim, et al., Mastocytosis-derived extracellular vesicles deliver miR-23a and miR-30a into pre-osteoblasts and prevent osteoblastogenesis and bone formation, Nat. Commun. 12 (1) (2021) 2527.

[34] G.-D. Lu, P. Cheng, T. Liu, Z. Wang, BMSC-derived exosomal miR-29a promotes angiogenesis and osteogenesis, Front. Cell Dev. Biol. 8 (2020) 608521.

[35] X. Yang, J. Yang, P. Lei, T. Wen, LncRNA MALAT1 shuttled by bone marrow-derived mesenchymal stem cells-secreted exosomes alleviates osteoporosis through mediating microRNA-34c/SATB2 axis, Aging (Albany NY) 11 (20) (2019) 8777–8791.

[36] Q. Dong, Z. Han, L. Tian, Identification of serum exosome-derived circRNA-miRNA-TF-mRNA regulatory network in postmenopausal osteoporosis using bioinformatics analysis and validation in peripheral blood-derived mononuclear cells, Front. Endocrinol. 13 (2022) 899503.

[37] M. Chen, Y. Li, H. Lv, P. Yin, L. Zhang, P. Tang, Quantitative proteomics and reverse engineer analysis identified plasma exosome derived protein markers related to osteoporosis, J. Proteomics 228 (2020) 103940.

[38] H. Shi, X. Jiang, C. Xu, Q. Cheng, MicroRNAs in serum exosomes as circulating biomarkers for postmenopausal osteoporosis, Front. Endocrinol. 13 (2022) 819056.

[39] C. Huang, Y. Wang, Downregulation of METTL14 improves postmenopausal osteoporosis via IGF2BP1 dependent posttranscriptional silencing of SMAD1, Cell Death Dis. 13 (11) (2022) 919.

[40] Y. You, J. Liu, L. Zhang, X. Li, Z. Sun, Z. Dai, et al., WTAP-mediated m6A modification modulates bone marrow mesenchymal stem cells differentiation potential and osteoporosis, Cell Death Dis. 14 (1) (2023) 33.

[41] Y. Xiong, Y. Zhang, F. Zhou, Y. Liu, Z. Yi, P. Gong, et al., FOXO1 differentially regulates bone formation in young and aged mice, Cell. Signal. 99 (2022) 110438.

[42] X. Ma, P. Su, C. Yin, X. Lin, X. Wang, Y. Gao, et al., The roles of FoxO transcription factors in regulation of bone cells function, Int. J. Mol. Sci. 21 (3) (2020).

[43] P. Chen, B. Hu, L.-Q. Xie, T.-J. Jiang, Z.-Y. Xia, H. Peng, Scara3 regulates bone marrow mesenchymal stem cell fate switch between osteoblasts and adipocytes by promoting Foxo1, Cell Prolif. 54 (8) (2021) e13095.

[44] Z. Fang, W. Mei, C. Qu, J. Lu, L. Shang, F. Cao, et al., Role of m6A writers, erasers and readers in cancer, Exp. Hematol. Oncol. 11 (1) (2022) 45.

[45] S. Zaccara, R.J. Ries, S.R. Jaffrey, Reading, writing and erasing mRNA methylation, Nat. Rev. Mol. Cell Biol. 20 (10) (2019) 608–624.

[46] X. Wang, B.S. Zhao, I.A. Roundtree, Z. Lu, D. Han, H. Ma, et al., N(6)-methyladenosine modulates messenger RNA translation efficiency, Cell 161 (6) (2015) 1388–1399.

[47] X. Wang, Z. Lu, A. Gomez, G.C. Hon, Y. Yue, D. Han, et al., N6-methyladenosine-dependent regulation of messenger RNA stability, Nature 505 (7481) (2014) 117–120.

[48] W. Xiao, S. Adhikari, U. Dahal, Y.-S. Chen, Y.-J. Hao, B.-F. Sun, et al., Nuclear m(6) A reader YTHDC1 regulates mRNA splicing, Mol. Cell 61 (4) (2016) 507–519.

[49] E. Rohner, R. Yang, K.S. Foo, A. Goedel, K.R. Chien, Unlocking the promise of mRNA therapeutics, Nat. Biotechnol. 40 (11) (2022) 1586–1600.

[50] P.S. Kowalski, A. Rudra, L. Miao, D.G. Anderson, Delivering the messenger: advances in technologies for therapeutic mRNA delivery, Mol. Ther. 27 (4) (2019) 710–728.